

# Wafer-scale on-chip synthesis and field emission properties of vertically aligned boron nitride based nanofiber arrays

Cite as: Appl. Phys. Lett. **114**, 093101 (2019); <https://doi.org/10.1063/1.5079655>

Submitted: 01 November 2018 • Accepted: 13 February 2019 • Published Online: 04 March 2019

 Hu Long, Thang Pham, Aiming Yan, et al.



View Online



Export Citation



CrossMark

## ARTICLES YOU MAY BE INTERESTED IN

[Low temperature wafer-scale synthesis of hexagonal boron nitride by microwave assisted surface wave plasma chemical vapour deposition](#)

AIP Advances **9**, 035043 (2019); <https://doi.org/10.1063/1.5091529>

[Boron nitride nanoscrolls: Structure, synthesis, and applications](#)

Applied Physics Reviews **6**, 021310 (2019); <https://doi.org/10.1063/1.5092547>

[Electron beam-induced nanopores in Bernal-stacked hexagonal boron nitride](#)

Applied Physics Letters **117**, 023102 (2020); <https://doi.org/10.1063/5.0010891>



## APL Quantum

CALL FOR APPLICANTS

Seeking Editor-in-Chief

# Wafer-scale on-chip synthesis and field emission properties of vertically aligned boron nitride based nanofiber arrays

Cite as: Appl. Phys. Lett. **114**, 093101 (2019); doi: [10.1063/1.5079655](https://doi.org/10.1063/1.5079655)

Submitted: 1 November 2018 · Accepted: 13 February 2019 ·

Published Online: 4 March 2019




View Online



Export Citation



CrossMark

Hu Long,<sup>1,2</sup>  Thang Pham,<sup>1,2,3</sup> Aiming Yan,<sup>1,2</sup> Zhen Guo,<sup>1</sup> Hiroya Ishida,<sup>4</sup> Wu Shi,<sup>1,2</sup> Sally Turner,<sup>1,2,5</sup> S. Matt Gilbert,<sup>1,2</sup> and Alex Zettl<sup>1,2,6,a)</sup>

## AFFILIATIONS

<sup>1</sup>Department of Physics, University of California at Berkeley, Berkeley, California 94720, USA

<sup>2</sup>Materials Sciences Division, Lawrence Berkeley National Laboratory, Berkeley, California 94720, USA

<sup>3</sup>Department of Materials Science and Engineering, University of California at Berkeley, Berkeley, California 94720, USA

<sup>4</sup>Sekisui Chemical Co. LTD, Shimamoto, Mishima, Osaka 618-0021, Japan

<sup>5</sup>Department of Chemistry, University of California at Berkeley, Berkeley, California 94720, USA

<sup>6</sup>Kavli Energy NanoScience Institute at the University of California, Berkeley and the Lawrence Berkeley National Laboratory, Berkeley, California 94720, USA

<sup>a)</sup>E-mail: [azettl@berkeley.edu](mailto:azettl@berkeley.edu)

## ABSTRACT

One dimensional boron nitride (BN) nanomaterials with a high aspect ratio are of great interest due to their unique properties and potential applications. However, BN nanomaterials are generally difficult to synthesize. Here, we describe the creation of arrays of vertically aligned pure BN nanofibers and BN coated carbon nanofibers, fabricated on-chip via a straightforward template-assisted chemical conversion reaction. The template, a glassy carbon nanofiber array, is produced by plasma processing of conventional photoresists. The method is highly controllable, patternable, and scalable, and the final arrays can be fabricated over large areas with a controlled fiber length. We characterize the electron field emission properties of the BN-coated carbon nanofiber array and find a large field enhancement factor, low turn-on voltage, and good stability. The outstanding field emission performance results from the small tip size and high aspect ratio of the nanofiber as well as the high chemical stability and high thermal conductivity of the BN coating.

Published under license by AIP Publishing. <https://doi.org/10.1063/1.5079655>

One-dimensional (1D) nanomaterials, such as nanotubes, nanowires, and nanofibers, have attracted significant interest due to their unique physical and chemical properties and a wide range of potential applications in photonics, electronics, sensors, and energy devices.<sup>1–6</sup> Hexagonal boron nitride (h-BN) is a structural analogue to carbon-based graphite, with alternating B and N atoms bonded into a hexagonal configuration.<sup>7</sup> Despite the structural similarity, BN is a wide bandgap insulator. This, together with other properties such as high thermal conductivity, high mechanical strength, and chemical and thermal resistance, makes 1D BN nanostructures highly desirable for many applications, including nanofillers in polymer composites for thermal management, hydrogen storage, and nanoscale electronic/optical devices.<sup>7–10</sup> Unfortunately, the synthesis of BN-based materials is generally complex, typically requiring high temperature and/or high

pressure. Hence, the creation of BN structures on-chip is particularly challenging.

Much effort has been devoted to the synthesis of BN nanotubes (BNNTs) since their initial discovery in 1995.<sup>11–19</sup> Multiple synthesis methods have been employed, including arc discharge, chemical vapor deposition, carbon nanotube conversion, laser vaporization, and inductively coupled plasma synthesis.<sup>12–19</sup> Far less attention has been paid to the development of 1D BN nanofibers (BNNFs) or nanowires (BNNWs). Nevertheless, the synthesis of BNNFs and BNNWs has yielded some encouraging results,<sup>20–23</sup> and the scalable creation of vertically aligned BNNFs on-chip would be a significant advance, especially if the orientation, dimensionality, and location of the nanofibers could be controlled.

Although there has been no previous report of a simple and scalable method for fabricating aligned BNNFs or BNNWs with

patterning capability, the fabrication of vertically aligned carbon nanomaterials, for instance, carbon nanotubes and carbon nanofibers, is well known. Vertically aligned carbon nanofibers (VACNFs) can be generated by a combination of oxygen plasma and high temperature pyrolysis, and such fiber arrays have been used for DNA bonding and supercapacitors.<sup>24–26</sup>

In this paper, we report a highly controllable method for the synthesis of related vertically aligned pure BNNF arrays and BN coated carbon nanofiber (BNCNF) arrays. Using plasma assisted photoresist-derived glassy carbon nanofiber arrays as templates, the carbon nanofibers are partly or fully converted to BN, thus forming BNCNFs or BNNFs, respectively. The method utilizes a standard photoresist as a starting material and the entire fabrication process is on-chip and compatible with CMOS fabrication processes. The nanofibers with a controlled length and diameter can thus be uniformly produced over large areas. The process is highly controllable, reproducible, and scalable. The field emission properties of the as-synthesized vertically aligned BNNFs and BNCNFs are also explored and found to be superior to those of more traditional CNT forests.

Figure 1(a) shows schematically the process flow for the fabrication of BNNF and BNCNF arrays. The process consists mainly of four critical steps: (i) standard lithography, (ii) oxygen plasma etching, (iii) carbonization, and (iv) BN coating or conversion. SU8, an epoxy-based negative photoresist which can be transformed into glass-like carbon microstructure at high temperature and in an inert atmosphere, is used as the starting material in the process and is patterned by UV exposure.<sup>24–28</sup> The SU8 is then treated by oxygen plasma to form an SU8 nanofiber array.<sup>24,25</sup> The typical scanning electron microscopy (SEM) images of the SU8 nanofiber are shown in Fig. S1. The formation of the polymer nanofiber array upon plasma etching is thought to be due to the directionality of the plasma etching combined with the self-masking effect brought about by the metal impurities (mainly antimony) in the polymer.<sup>24–26,29,30</sup> Pyrolysis is performed by heating the sample to 900 °C under nitrogen and keeping it at 900 °C for 2 h to yield carbon nanofibers (CNFs). The temperature control curve is shown in Fig. S2. The nanofiber morphology is well preserved with around 50% shrinkage in both the length and the diameter

during the carbonization process. The CNFs are then coated with BN or fully converted to BNNFs by a carbothermal reduction method, utilizing boric acid powder and ammonia gas as boron and nitrogen sources, respectively. This reaction has been previously used to convert graphene into h-BN or forming coatings on carbon nanotubes at low temperature.<sup>16,31–33</sup>

Using ammonia as a reaction gas instead of nitrogen is also effective, and this can significantly decrease the carbon substitution reaction temperature. In this case, the glassy carbon fiber array is loaded into the high temperature zone of the furnace and heated to a high temperature of 1000–1200 °C with ammonia flow (100 sccm) for 20 min, while boric acid in the low temperature zone is heated to 500 °C. During the reaction, boron and nitrogen atoms gradually replace carbon atoms and form h-BN. Based on the reaction temperature and time, the carbon nanofibers can be either BN-coated or fully converted to BNNFs.

Figures 1(b) and 1(c) show top- and edge-view low magnification scanning electron microscopy (SEM) images of a vertically aligned BNNF array uniformly distributed on a silicon chip over a large area, respectively.

The morphologies of the CNFs, BNCNFs, and BNNFs are further studied by SEM and transmission electron microscopy (TEM). As shown in Figs. 2(a), 2(b), and S3, the CNFs have a diameter of around 5–200 nm. As shown by the low magnification TEM image in Fig. S4, the CNFs are branched and slightly interconnected (sometimes more at their tips). The CNFs are mainly amorphous although some graphitic ribbon-like structure exists, in good agreement with previous studies on glassy carbon.<sup>24–27</sup> The fiber length is controlled by the thickness of the initial SU8 layer and the plasma treatment time. Longer plasma treatment time allows etching deeper into the SU8 layer, thus leading to longer nanofibers. As shown in Fig. S3, the length of the CNFs increases from 1.35 to 4.1 μm as the plasma treatment time increases from 300 to 600 s. The nanofibers are connected by a carbon layer underneath which is derived from the unetched SU8 layer. The thickness of this layer can also be controlled during the plasma treatment.

The fiber morphology and vertical alignment are faithfully retained after the conversion reaction (see Fig. 2). No obvious fiber length change is observed for all synthesis conditions. Figures 2(c) and 2(d) show SEM and TEM images of BNCNFs obtained from a partial conversion reaction performed at 1000 °C. For partial conversion, the BNCNFs have overall diameters similar to those of the original CNFs. As is apparent in the upper part of Fig. 2(d), in the partial conversion process, a thin layer of crystalline material forms at the surface of the amorphous carbon fiber, reflecting the formation of a BN layer. After a conversion reaction at 1200 °C, the nanofibers show a complete graphitic structure, and the carbon fibers have been fully converted to pure BNNFs. For such a complete conversion, the diameter of the fibers is increased to 20–300 nm (see Fig. S5).

The composition before and after the conversion reaction is identified by Raman, Fourier-transform infrared spectroscopy (FTIR), and electron energy loss spectroscopy (EELS), as shown in Fig. 3. Raman spectra of CNFs show broad D and G peaks at 1352 and 1602 cm<sup>-1</sup>. Characteristic D and G peaks are also observed for the BNCNFs, which confirms that the glassy carbon structure of CNFs is not altered by the partial conversion. For BNCNFs, the coexistence of a D mode from glassy carbon and an E<sub>2g</sub> mode from h-BN results in a peak at

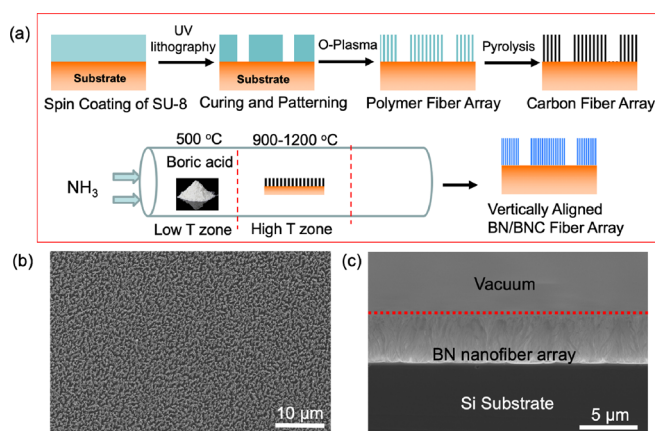


FIG. 1. (a) Schematic of the fabrication process flow for aligned BNNF and BNCNF arrays. (b) and (c) SEM images of the BN nanofiber array on the Si substrate over large area: (b) top view and (c) side view.

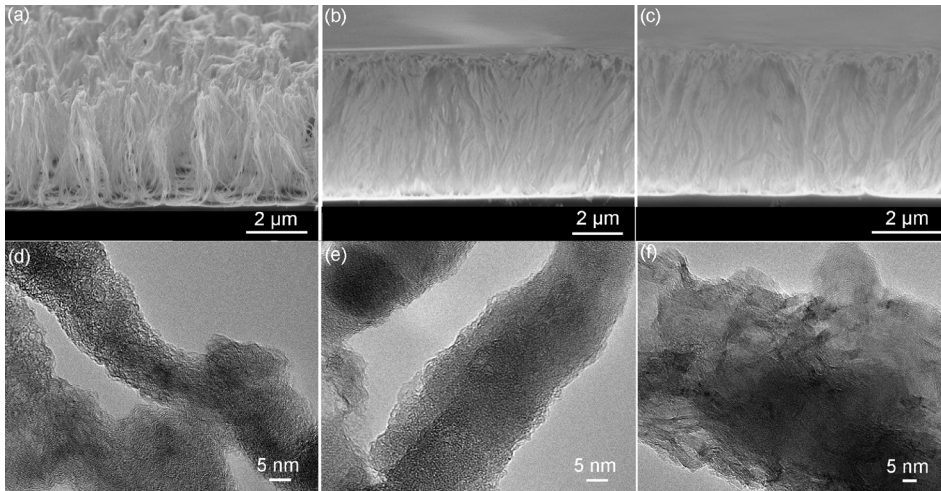


FIG. 2. SEM and TEM images of (a) and (b) CNFs, (c) and (d) BNCNFs, and (e) and (f) BNNFs.

$1362\text{ cm}^{-1}$ , with enhanced intensity compared to the D peak from Raman spectra of CNFs. For the fully converted BNNFs, only a relatively weak peak located at  $1366\text{ cm}^{-1}$  is found, which is related to the  $E_{2g}$  mode of h-BN. The absence of D and G modes in Fig. 3(a) demonstrates the complete conversion from glassy carbon to BN. Figure 3(b) shows the FT-IR spectra of CNFs, BNCNFs, and BNNFs. The curves for BNCNF and BNNF show the characteristic B-N and B-N-B stretching at around  $1377$  and  $788\text{ cm}^{-1}$ , respectively. The observation further confirms the existence of BN in BNCNFs and BNNFs, while no such peak is found for CNFs.

TEM-EELS is also used to determine the presence of B, C, and N elements in the nanofibers, as shown in Figs. 3(c) and 3(d). For both BNCNFs and BNNFs, adsorption peaks located at 193 and 403 eV appear in the EELS spectrum, which correspond to B-K and N-K edges, respectively, confirming the B-N bonding. In addition, an adsorption peak located at 282 eV, corresponding to the  $sp^2$  C-C

bond, is observed in BNCNFs, indicating the coexistence of both BN and carbon networks in the same BNCNF.

It is well known that nanostructured carbon materials may be suitable for use as field emission sources due to favorable turn-on voltages and high emission currents, leading to applications ranging from flat-panel displays and X-ray sources to microwave amplifiers.<sup>4,34–36</sup> A wide range of carbon based field emitters, such as carbon nanotubes, doped diamond, and diamond-like carbon (DLC), have been extensively studied.<sup>37–40</sup> For example, carbon nanotube based emitters are attractive due to their unique needle-like nanostructure with associated tip “field amplification” and their high electric conductivity.<sup>4,34–37</sup> There are also reports of using glassy carbon as field emitting materials.<sup>41–44</sup> However, glassy carbon materials are difficult to engineer into a sharp tip structure, which limits their field emitting performance. In addition, carbon materials by themselves degrade very easily due to their tendency to burn out and their high sensitivity to oxygen during emission. To address these problems, the combination of carbon materials with wide bandgap materials (WBG) has been considered.<sup>31,45–47</sup> The WBG coating in this case has two functions: 1. As a protective layer for the conductive core to prevent or minimize emission instabilities from adsorption of residual gas molecules. 2. With the right thickness, WBG can decrease the effective work function of emitters, resulting in better emission performance.<sup>31,45,46</sup>

The field emission properties of vertically aligned CNFs, vertically aligned BNCNFs, and vertically aligned BNNFs are here explored and compared to the more conventional vertically aligned CNT forest. Figure 4(a) shows the schematic of the emission measurement setup, which is a simple diode configuration with a metal anode of 3.2 mm in diameter under high vacuum ( $\sim 3 \times 10^{-8}$  Torr). The dependencies of the field emission current on the electric field are shown in Fig. 4(b). We do not plot current density because of the large density difference between the nanofiber array and the CNT forest. The turn-on field is defined as the electric field required to generate a current of  $0.8\text{ }\mu\text{A}$  for the device (corresponding to a current density of  $10\text{ }\mu\text{A}/\text{cm}^2$  averaged over the entire sample area). The average turn on fields for vertically aligned CNFs and vertically aligned CNTs are found to be similar, around  $2.1\text{ V}/\mu\text{m}$ , while the turn on field is  $2.5\text{ V}/\mu\text{m}$  for vertically aligned BNCNFs. The turn on fields obtained here are much lower

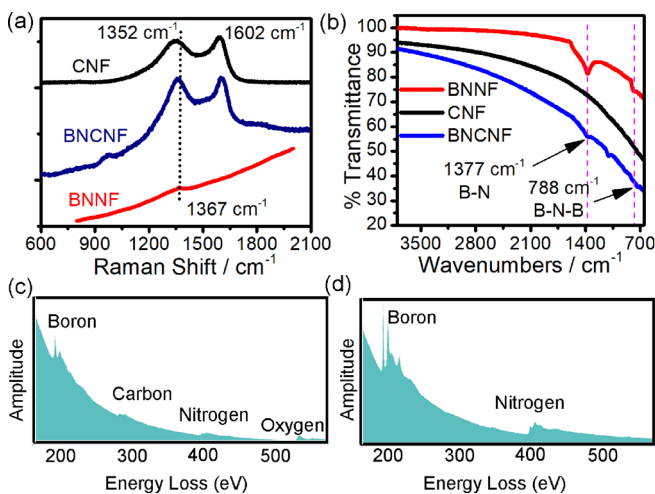
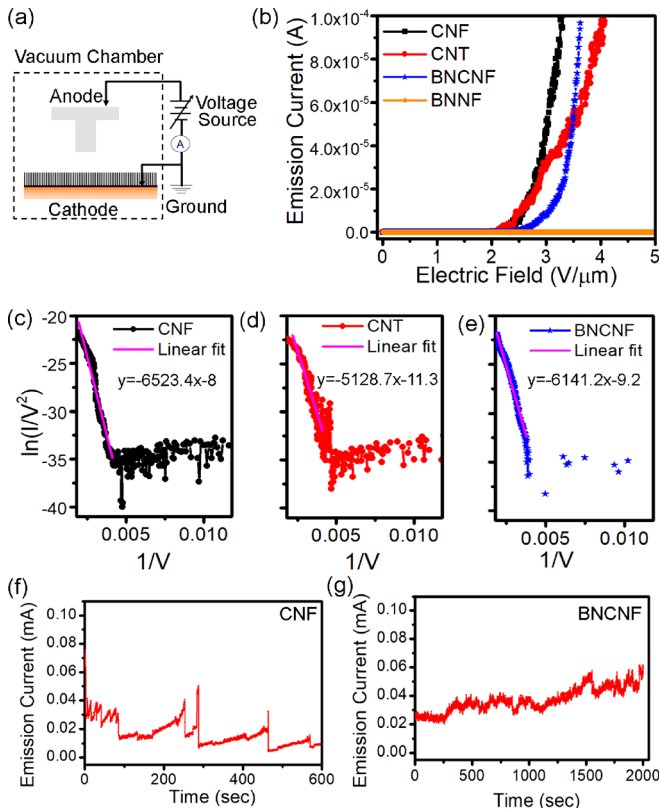


FIG. 3. (a) Raman spectra of the fiber array obtained at different reaction temperatures. (b) FTIR spectra of the fiber arrays (c) and (d) EELS spectra of (c) BNCNFs and (d) BNNFs.



**FIG. 4.** Field emission properties. (a) Field emission measurement setup. (b) Emission current vs electric field. (c)–(e) FN plot of CNFs, CNTs, and BNCNFs. (f) and (g) Emission stability of CNFs and BNCNFs at 3 V/μm.

compared to previously reported glassy carbon emitters, and similar to CNTs.<sup>31,33,35–37,43–45</sup> No emission current is observed for vertically aligned BNNF in our voltage range, which is expected as BNNFs are not conducting.

Figures 4(c)–4(e) show the corresponding  $\ln(I/V^2)$  versus  $1/V$  plots of vertically aligned CNFs, vertically aligned CNTs, and vertically aligned BNCNFs, respectively, representing the traditional Fowler-Nordheim (FN) tunneling plot. All the FN plots presented here can be reasonably fitted to straight lines, as expected for an electron field emission process. As per the FN equation, the emitted current density is given by

$$J = \frac{A\beta^2 E^2}{\phi} \exp\left(\frac{-B\phi^{3/2}}{\beta E}\right), \quad (1)$$

where  $J = I/a$  is the emission current density, in which  $I$  is the emission current and  $a$  is the effective area,  $A = 1.56 \times 10^{-6} \text{ A V}^{-2} \text{ eV}$ ,  $B = 6.83 \times 10^3 \text{ eV}^{-3/2} \text{ V } \mu\text{m}^{-1}$ ,  $\phi$  is the work function,  $E = V/d$  is the applied field, in which  $V$  is applied voltage and  $d$  is the spacing between the anode and the cathode, and  $\beta$  is the field enhancement factor. Equation (1) can be written as

$$\ln\left(\frac{I}{V^2}\right) = \left(-\frac{B\phi^{3/2}}{\beta/d}\right)\left(\frac{1}{V}\right) + \ln\left(\frac{A_*}{\phi}\left(\frac{\beta}{d}\right)^2 * a\right). \quad (2)$$

Consequently, the field enhancement factors of can be calculated from the slope of the linear curve as

$$S = -\frac{B\phi^{3/2}}{\beta/d}. \quad (3)$$

The work function of glassy carbon is taken to be similar to that of CNTs, that is, 5 eV.<sup>45–47</sup> We thus find the field enhancement factors of CNFs and CNTs to be 1849 and 2011, respectively. Such field enhancement factors are in the reported range for CNTs and much higher than those reported for glassy carbon emitters.<sup>31,33–36,42–44,48</sup>

The large field enhancement factor primarily arises from the small tip size of the nanofiber formed by plasma etching. As the h-BN coating on CNFs is very thin, the emitter tip radius is assumed to be not changed; thus, the field enhancement factor is assumed the same for BNCNFs. Using this assumption, the calculated work function of the BNCNFs is 5.02 eV, which is slightly higher than that of CNFs. The result is consistent with the insulating nature of h-BN, which increases the tunneling barrier.

We also perform stability tests, to evaluate the emission current as a function of time while maintaining an electric field of 3 V/μm, as shown in Figs. 4(f) and 4(g). The stability of the BN coated emitter is greatly improved over that of the bare CNF emitter. The improved stability can be ascribed to the excellent structural stability and the high oxidation resistance of the h-BN coating.

In summary, we present a method for the on-chip fabrication of vertically aligned BNNFs and BNCNFs with good uniformity. This method is scalable and controllable, which complements the fabrication methods for nanostructured BN and BN-carbon hybrid materials. Nanofibers with a controlled morphology and composition are fabricated. The fabricated nanofibers can be potentially used in many applications, such as thermal interface materials and field emitters. The field emission properties of the nanofibers are investigated. The obtained results are superior to those of other glassy carbon based emitters and comparable to CNT based emitters. The results suggest that the as-fabricated BNCNFs may be excellent field emitters with a low turn on voltage, large field enhancement factor, high current density, and good long-term stability.

**Fabrication of the carbon nanofiber array:** Si (100) wafers (p-type, doped, 1000 Ω/cm<sup>2</sup>, 500 μm thick) are used as a substrate and cleaned with acetone, IPA, and water before using. In a typical process, an SU8 2000 resist (MicroChem Corp.) is spin coated onto the cleaned substrate at 4000 rpm for 60 s. The thickness of the obtained film is controlled by changing the spin coating conditions. The sample is then baked at 65 °C for 5 min and 90 °C for 10 min. Next, the sample is exposed to UV for patterning as well as crosslinking the polymer. After a baking at 65 °C and 95 °C, the sample is cooled down to room temperature. Then, the sample is treated with oxygen plasma (Plasma etcher) with a power of 250 W, 50 sccm O<sub>2</sub> flow for different amounts of time, resulting in nanofiber arrays. Then, the sample is subjected to a pyrolysis process at 900 °C for 2 h under a nitrogen environment, and the temperature control curve is shown in Fig. S2.

**Fabrication of BN and BNC nanofibers:** The conversion reaction is carried out in a quartz tube furnace. The carbon fiber on Si is loaded into the high temperature zone of the furnace and boric acid is loaded in the low temperature zone. The tube is pumped down to ~10 mTorr and then flushed with 100 sccm nitrogen (N<sub>2</sub>) gas for 10 min. Then, the furnace is heated to 1000 °C to 1200 °C in 30 min and kept at this

temperature. At the same time, boric acid is heated to 500 °C by a heating tape. Meanwhile, 100 sccm ammonia (NH<sub>3</sub>) is introduced to the tube, replacing the N<sub>2</sub> gas. After reaction for 30 min, the sample is taken out and washed by 80 °C hot water to remove the boron oxide residues. The reaction can be controlled as coating or conversion by conversion temperature. At 1000 °C, a BN coated CNF array is obtained, while a BNNF array can be obtained at 1200 °C.

See [supplementary material](#) for SEM images of the SU8 nanofiber array, temperature control curve for the carbonization process, cross sectional SEM images of the carbon fiber array obtained with different plasma times, and low magnification TEM images of the carbon nanofibers and BN nanofibers.

This work was supported in part by the Director, Office of Science, Office of Basic Energy Sciences, Materials Sciences and Engineering Division, of the U.S. Department of Energy under Contract No. DE-AC02-05-CH11231, within the sp<sup>2</sup>-Bonded Materials Program (KC2207), which provided for synthesis and SEM characterization of the nanofibers, and within the Van der Waals Heterostructures Program (KCWF16), which provided for Raman and FTIR characterization. Support was also provided by the National Science Foundation under Grant No. 1542741, which provided for field emission testing, and under Grant No. DMR-1807233 which provided for TEM characterization. SMG acknowledges funding from NSF GRFP and the Kavli ENSI Philomathia Graduate Fellowship.

## REFERENCES

- <sup>1</sup>S. Iijima, *Nature* **354**, 56 (1991).
- <sup>2</sup>T. Zhai, L. Li, Y. Ma, M. Liao, X. Wang, X. Fang, J. Yao, Y. Bando, and D. Golberg, *Chem. Soc. Rev.* **40**, 2986 (2011).
- <sup>3</sup>Y. Cui, C. M. Lieber, and M. G. Bawendi, *Science* **291**, 851 (2001).
- <sup>4</sup>P. G. Collins and A. Zettl, *Appl. Phys. Lett.* **69**, 1969 (1996).
- <sup>5</sup>P. G. Collins, *Science* **287**, 1801 (2000).
- <sup>6</sup>S. Fan, M. G. Chapline, N. R. Franklin, T. W. Tomblor, A. M. Cassell, and H. Dai, *Science* **283**, 512 (1999).
- <sup>7</sup>J. Yin, L. Jidong, Y. Hang, Y. Jin, G. Tai, L. Xuemei, Z. Zhang, and W. Guo, *Small* **12**, 2942 (2016).
- <sup>8</sup>D. Golberg, Y. Bando, C. C. Tang, and C. Y. Zhi, *Adv. Mater.* **19**, 2413 (2007).
- <sup>9</sup>D. Golberg, Y. Bando, Y. Huang, T. Terao, M. Mitome, and C. Tang, *ACS Nano* **4**, 2979 (2010).
- <sup>10</sup>C. Tang, Y. Bando, X. Ding, A. S. Qi, and D. Golberg, *J. Am. Chem. Soc.* **124**, 14550 (2002).
- <sup>11</sup>N. G. Chopra, R. J. Luyken, K. Cherrey, V. H. Crespi, M. L. Cohen, S. G. Louie, and A. Zettl, *Science* **269**, 966 (1995).
- <sup>12</sup>A. Loiseau, F. Willaime, N. Demoncy, G. Hug, and H. Pascard, *Phys. Rev. Lett.* **76**, 4737 (1996).
- <sup>13</sup>J. Cumings and A. Zettl, *Chem. Phys. Lett.* **316**, 211 (2000).
- <sup>14</sup>C. H. Lee, M. Xie, V. Kayastha, J. Wang, and Y. K. Yap, *Chem. Mater.* **22**, 1782 (2010).
- <sup>15</sup>W. Han, Y. Bando, K. Kurashima, and T. Sato, *Appl. Phys. Lett.* **73**, 3085 (1998).
- <sup>16</sup>R. Y. Tay, H. Li, S. H. Tsang, L. Jing, D. Tan, M. Wei, and E. H. T. Teo, *Chem. Mater.* **27**, 7156 (2015).
- <sup>17</sup>Y. Chen, J. Fitz Gerald, J. S. Williams, and S. Bulcock, *Chem. Phys. Lett.* **299**, 260 (1999).
- <sup>18</sup>A. Fathalizadeh, T. Pham, W. Mickelson, and A. Zettl, *Nano Lett.* **14**, 4881 (2014).
- <sup>19</sup>K. S. Kim, C. T. Kingston, A. Hrdina, M. B. Jakubinek, J. Guan, M. Plunkett, and B. Simard, *ACS Nano* **8**, 6211 (2014).
- <sup>20</sup>K. F. Huo, Z. Hu, F. Chen, J. J. Fu, Y. Chen, B. H. Liu, J. Ding, Z. L. Dong, and T. White, *Appl. Phys. Lett.* **80**, 3611 (2002).
- <sup>21</sup>X. Zhang, G. Lian, H. Si, J. Wang, D. Cui, and Q. Wang, *J. Mater. Chem. A* **1**, 11992 (2013).
- <sup>22</sup>J. Lin, L. Xu, Y. Huang, J. Li, W. Wang, C. Feng, Z. Liu, X. Xu, J. Zou, and C. Tang, *RSC Adv.* **6**, 1253 (2016).
- <sup>23</sup>Y. J. Chen, B. Chi, D. C. Mahon, and Y. Chen, *Nanotechnology* **17**, 2942 (2006).
- <sup>24</sup>D. Volder, M. F. L. Vansweevelt, R. Wagner, P. Reynaerts, D. Van Hoof, C. Hart, and A. John, *ACS Nano* **5**, 6593 (2011).
- <sup>25</sup>S. Jiang, T. Shi, Y. Gao, H. Long, S. Xi, and Z. Tang, *J. Micromech. Microeng.* **24**, 045001 (2014).
- <sup>26</sup>S. Jiang, T. Shi, X. Zhan, S. Xi, H. Long, B. Gong, J. Li, S. Cheng, Y. Huang, and Z. Tang, *J. Micromech. Microeng.* **25**, 113001 (2015).
- <sup>27</sup>H. Long, S. Xi, D. Liu, T. Shi, Q. Xia, S. Liu, and Z. Tang, *Opt. Express* **20**, 17126 (2012).
- <sup>28</sup>H. Long, T. Shi, S. Xi, F. Wu, Q. Xia, X. Li, and Z. Tang, *Int. J. Nanotechnol.* **11**, 616 (2014).
- <sup>29</sup>J. R. Morber, X. Wang, J. Liu, R. L. Snyder, and Z. L. Wang, *Adv. Mater.* **21**, 2072 (2009).
- <sup>30</sup>H. Fang, W. Wu, J. Song, and Z. L. Wang, *J. Phys. Chem. C* **113**, 16571 (2009).
- <sup>31</sup>X. Yang, Z. Li, F. He, M. Liu, B. Bai, W. Liu, X. Qiu, H. Zhou, C. Li, and Q. Dai, *Small* **11**, 3710 (2015).
- <sup>32</sup>Y. Gong, G. Shi, Z. Zhang, W. Zhou, J. Jung, W. Gao, L. Ma, Y. Yang, S. Yang, G. You, R. Vajtai, Q. Xu, A. H. Macdonald, B. I. Yakobson, J. Lou, Z. Liu, and P. M. Ajayan, *Nat. Commun.* **5**, 3193 (2014).
- <sup>33</sup>W. A. de Heer, A. Châtelain, and D. Ugarte, *Science* **270**, 1179 (1995).
- <sup>34</sup>K. B. K. Teo, M. Chhowalla, G. A. J. Amaratunga, W. I. Milne, G. Pirio, P. Legagneux, F. Wyczisk, D. Pribat, and D. G. Hasko, *Appl. Phys. Lett.* **80**, 2011 (2002).
- <sup>35</sup>Z. Liu, G. Yang, Y. Z. Lee, D. Bordelon, J. Lu, and O. Zhou, *Appl. Phys. Lett.* **89**, 103111 (2006).
- <sup>36</sup>W. I. Milne, K. B. K. Teo, G. A. J. Amaratunga, P. Legagneux, L. Gangloff, J.-P. Schnell, V. Semet, V. Thien Binh, and O. Groening, *J. Mater. Chem.* **14**, 933 (2004).
- <sup>37</sup>S. H. Jo, D. Z. Wang, J. Y. Huang, W. Z. Li, K. Kempa, and Z. F. Ren, *Appl. Phys. Lett.* **85**, 810 (2004).
- <sup>38</sup>G. A. J. Amaratunga and S. R. P. Silva, *Appl. Phys. Lett.* **68**, 2529 (1996).
- <sup>39</sup>M. Tanemura, J. Tanaka, K. Itoh, Y. Fujimoto, Y. Agawa, L. Miao, and S. Tanemura, *Appl. Phys. Lett.* **86**, 113107 (2005).
- <sup>40</sup>H. Zanin, P. W. May, M. H. M. O. Hamanaka, and E. J. Corat, *ACS Appl. Mater. Interfaces* **5**, 12238 (2013).
- <sup>41</sup>S. Yamamoto, S. Hosoki, S. Fukuhara, and M. Futamoto, *Surf. Sci.* **86**, 734 (1979).
- <sup>42</sup>M. Deguchi and A. Taomoto, *Vacuum* **84**, 438 (2009).
- <sup>43</sup>V. I. Shesterkin, T. N. Sokolova, S. P. Morev, D. A. Bessonov, E. L. Surmenko, A. N. Darmaev, D. A. Komarov, E. K. Murav'ev, P. D. Shalaev, and K. V. Shumikhin, *J. Commun. Technol. Electron.* **61**, 1044 (2016).
- <sup>44</sup>Y. Tzeng, C. Liu, and A. Hirata, *Diamond Relat. Mater.* **12**, 456 (2003).
- <sup>45</sup>V. V. Zhimov, W. B. Choi, J. J. Cuomo, and J. J. Hren, *Appl. Surf. Sci.* **94/95**, 123 (1996).
- <sup>46</sup>W. K. Yi, T. W. Jeong, S. G. Yu, J. N. Heo, C. S. Lee, J. H. Lee, W. S. Kim, J.-B. Yoo, and J. M. Kim, *Adv. Mater.* **14**, 1464 (2002).
- <sup>47</sup>D. Kang, V. V. Zhirnov, R. C. Sanwald, J. J. Hren, and J. J. Cuomo, *J. Vac. Sci. Technol. B* **19**, 50 (2001).
- <sup>48</sup>R. H. Baughman, A. A. Zakhidov, and W. A. de Heer, *Science* **297**, 787 (2002).